CHAPTER 29

Microsphere contrast agents for OCT

Stephen A Boppart Kenneth S Suslick

INTRODUCTION

Contrast agents are utilized in virtually every imaging modality to enhance diagnostic capabilities. In addition, when imaging biological tissues, it is often desirable to enhance the signals measured from specific, labeled molecular structures, such as cell receptors. This is central to the emerging field of molecular imaging. Contrast agents which produce a specific image signature have been utilized in imaging modalities including ultrasound[1], computed tomography[2], magnetic resonance imaging[3], and optical microscopy[4], among many others. In addition, the identification of molecular targets and the development of strategies for labeling these targets have received increasing attention. For optical imaging, the majority of molecularly targeted probes have been based on fluorescence or bioluminescence. However, optical imaging technologies insensitive to inelastically scattered light, such as OCT[5] or reflectance confocal microscopy, must rely on other fundamental changes in optical properties, namely changes in scattering, absorption, or polarization, or rely on a time- or frequency-dependent modulation of amplitude, phase, or frequency of the light.

OCT has found application in a wide range of biological and medical applications[6–10]. Given the ability of OCT to perform high-resolution three-dimensional imaging at remote sites, the use of OCT in cardiovascular applications has been a major focus of research and is likely to be a primary application area in highly scattering tissues, such as within human coronary arteries[11]. Scenarios exist for which contrast agents could improve our ability to identify cardiovascular pathologies. A number of vascular endothelial markers are expressed during atherosclerosis and in angiogenesis; these include various integrin receptors (specifically the $\alpha_v\beta_3$ receptor), which have been targeted by many investigators in many studies, and across numerous imaging modalities[12–14]. To date, no contrast agents are routinely used to enhance the diagnostic utility of OCT or to label and thereby specifically identify

molecular-level features within OCT images. In recent years, there has been an increased interest in achieving this goal for OCT[15], with the development of contrast agents such as microspheres[16,17], absorbing dyes[18,19], plasmon-resonant nanoparticles[20,21] and magnetomotive nanoparticles[22]. This chapter describes the fabrication, characterization and application of a new class of engineered protein microsphere optical contrast agents that are not based on fluorescence, but rather on scattering or absorbing nanoparticles within the shell or core. These agents are suitable for reflection- or scattering-based optical imaging techniques, such as OCT, but also include light and reflectance confocal microscopy. These agents are biocompatible[23], are suitable for *in vivo* use, and produce enhanced backscatter that is detectable in highly scattering tissue. These agents may be tailored to adhere to specific molecules, cells, or tissue types and thus provide additional selectivity that can enhance the utility of OCT as an emerging diagnostic technique.

A precedent for scattering-based protein-shelled microspheres exists for cardiovascular ultrasound imaging. Air- or perfluorocarbon-filled microspheres[24] have been used as scattering echogenic contrast agents to enhance the blood–tissue contrast within the cardiovascular system[25] and, more recently, for identifying tumor vasculature[26]. Since OCT detects scattering changes, this goal can be achieved by delivering highly scattering contrast agents into the tissue and allowing the agents to attach to specific regions of interest. This chapter focuses on the progress and application of engineered optical contrast agents that are microspheres 0.2–5 μm in diameter with an approximately 50 nm-thick protein shell. The microspheres are designed to incorporate in their shell and encapsulate in their core a wide range of nanoparticles and materials which alter the local optical properties of tissue. The protein shell may also be functionalized to target the agents to specific regions of interest.

Contrast agents designed for efficient light scattering are sensed either directly by detecting their scattered light or indirectly through their attenuation of the incident light. Imaging modalities such as OCT are based on detecting backscattering and operate in the 'biological window' of near-infrared wavelengths where absorption is minimal and attenuation is governed primarily by scattering. To alter the intensity of backscattered light in OCT, scattering contrast agents must introduce a local region of change in index of refraction. For instance, even the introduction of air into tissue produces a significant change in index, thereby increasing the intensity of the backscattered light in OCT. One of the first demonstrations of scattering contrast agents was the use of gold nanoparticles in electron microscopy to label specific regions within cells[27]. Commercially available air-filled (Albunex®) and perfluorocarbon-filled albumin microspheres for use as contrast-enhancing agents in ultrasound[24] were also used to enhance optical contrast in OCT[16]. With recent advances in sonochemistry and chemical modification of probes, a wide variety of engineered microspheres have been fabricated to optimize the optical scattering properties of these contrast agents[17].

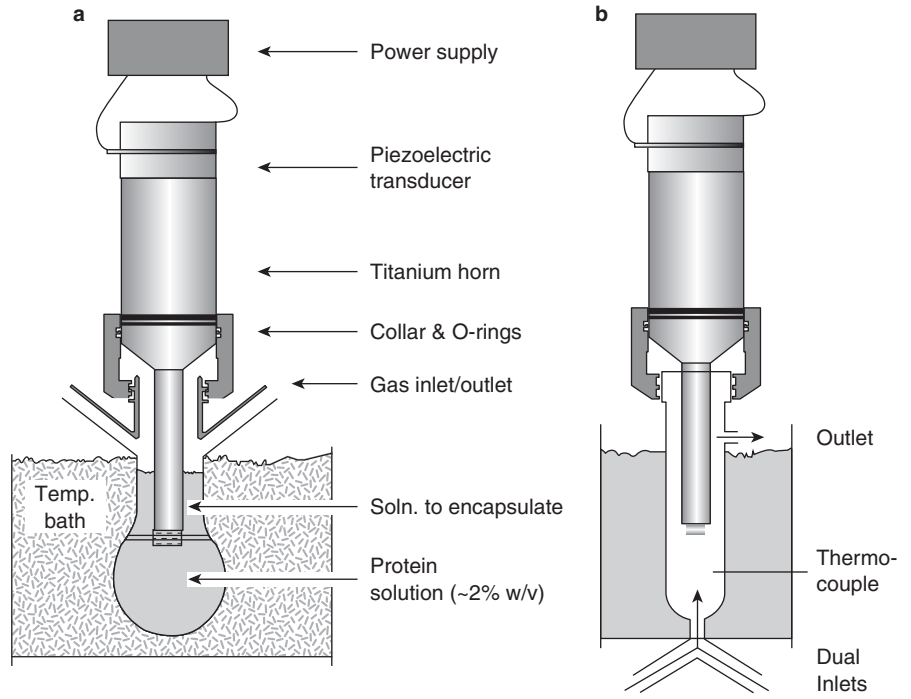

Figure 29.1 Fabrication hardware. Standard ultrasonic horns have been used to develop both batch (A) and flow reactors (B) for the preparation of protein-shelled microspheres

FABRICATION CHEMISTRY

Using high-intensity ultrasound and simple protein solutions, a sonochemical method (Figure 29.1) to make both air-filled microbubbles and non-aqueous liquid-filled microspheres (microcapsules) has been developed[28]. These microspheres are stable for months. They are smaller than erythrocytes, and thus are able to pass unimpeded through, but not out of, the circulatory system. Examined by optical microscopy, scanning and transmission electron microscopy, and particle counting, batches of microspheres exhibit narrow Gaussian-shaped size distributions (Figure 29.2, average diameter, $2.5 \pm 1.0\,\mu m$). While the protein shells are quite thin (~50 nm, e.g. ~8 protein molecules across) and gas permeable, the spheres are physically robust and survive filtration and centrifugation.

Early studies have delineated the mechanism responsible for protein-shell microsphere formation[28,29]. It is, in fact, a combination of two acoustic phenomena: emulsification and cavitation. Ultrasonic emulsification creates the microscopic dispersion of the air or non-aqueous phase into the protein

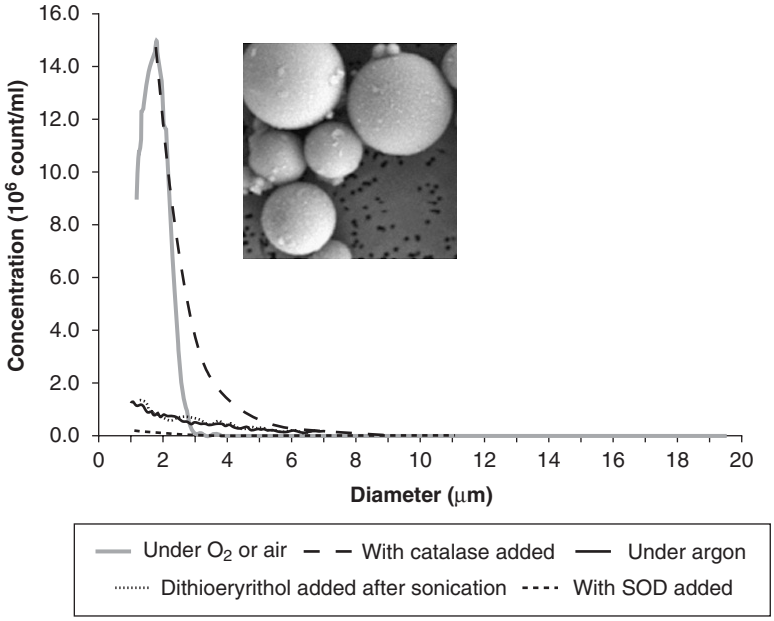

Figure 29.2 Microsphere size distributions. Particle (Coulter Multisizer) counts of bovine serum albumin microspheres in the presence of trapping agents. Narrow Gaussian-like distributions are typical. Size ranges are commonly $2.5 \pm 1.0\,\mu m$, depending on ultrasound acoustic energy. Inset is a scanning electron micrograph of a collection of microspheres. SOD, superoxide dismutase

solution necessary to form the protein microcapsules. Alone, however, emulsification is insufficient to produce long-lived microspheres. For example, emulsions produced by vortex mixing produce no long-lived microspheres.

As shown in Figure 29.2, microcapsule formation is strongly inhibited by the absence of O_2, by free radical traps, by superoxide dismutase (but not by catalase), and by the lack of (or protection of) free cysteine residues in the protein. Cysteine residues can be both oxidized and disulfides reduced by sonochemically produced superoxide[30]; this creates interprotein disulfide bonds that cross-link the proteins and hold the protein-shell microspheres together[28,29]. To confirm the presence of disulfide bonds within the sonochemically generated microspheres, samples of native bovine serum albumin (BSA), BSA-shell microspheres, and BSA-shell microspheres pre-reduced for increasing lengths of time with the disulfide cleaving agent dithioerythritol (DTE, a standard disulfide reductant) were examined on a non-denaturing polyacrylamide gel electrophoresis (PAGE) gel. BSA microspheres without DTE pretreatment showed no detectable bands, indicating the lack of free BSA or oligomers in our purified microspheres. BSA microspheres exposed to DTE for various time periods (from 3 minutes to 13 hours) showed degradation to

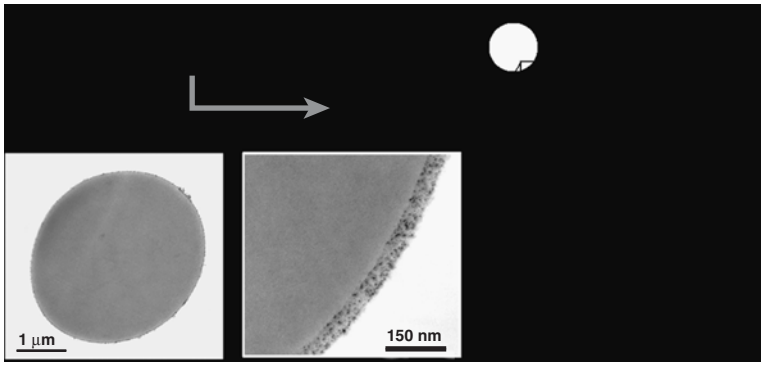

Figure 29.3 Fabrication chemistry. Aqueous sonochemistry produces homolysis of water. In the presence of oxygen, the hydrogen atoms are converted to hydroperoxyl (HO_2, i.e. protonated superoxide). Superoxide can both scramble cysteine disulfide bonds and oxidize free cysteine to form new disulfide crosslinks. A schematic view of the disulfide crosslinking of the protein molecules making up the shell of the microspheres is shown. As measured by transmission electron microscopy, the crosslinked protein shell is ~ 50 nm (i.e. ~ 8 bovine serum albumin molecules) thick. Note the availability of surface functionality for conjugation and surface modification

oligomers, tetramers, trimers, dimers and monomers. As the length of DTE treatment increased, a strong decrease in the amount of oligomers and a strong increase in the concentration of dimers and monomers was observed. As illustrated in Figure 29.3, protein cysteine residues are oxidized during microsphere formation by sonochemically produced superoxide.

Ultrasonic irradiation of liquids produce acoustic cavitation: the formation, growth and implosive collapse of bubbles. The collapse of such bubbles creates transient hot-spots with enormous peak temperatures[31]. Sonolysis of water is known to produce H , OH , H_2, H_2O_2, and, in the presence of oxygen, superoxide (O_2^-), or in its protonated form, hydroperoxyl (HO_2)[32]. Superoxide creates interprotein disulfide bonds that cross-link the proteins and hold the microbubbles together (Figure 29.3). This dispersion of gas or non-aqueous liquid into the protein solution, coupled with chemical cross-linking of the protein at the bubble interface, results in the formation of long-lived protein-shell microspheres filled with air or non-aqueous liquid.

Given the extreme conditions generated during cavitation[31], it may at first glance appear surprising that the protein of our protein microspheres remains intact. Note, however, that the extreme conditions during cavitation are inside the gas phase of the collapsing bubble and therefore do not affect the protein directly. After all, the protein molecules are dissolved out in the bulk liquid phase of the solution. Second, the cross-linking of cysteine residues is not unusual and need not affect function dramatically; for example, *in vivo*, several per cent of the serum albumin is dimerized by interprotein disulfide bonds[30].

Table 29.1 Combinations of engineered microsphere shells, cores and surface modifications

Protein shells	*Inner cores*	*Surface modifications*
Albumin	Air, O_2, N_2, Ar	PEG, RGD peptide
Hemoglobin	Vegetable oils	Fluorescein
Pepsin	Water	Au, Fe_2O_3 colloids
Immunoglobulins	Organic liquids	Immunoglobulins
Lipase	Ferrofluids	Folate
Peroxidases	Fluorocarbons	Gd complexes
Polymers	Iodinated agents	Antibodies
	Gd complexes	Carbon
		Melanin

Fabrication protocols have been developed to enable variation of microsphere size, shell or encapsulated material, and surface protein features (Table 29.1, Figure 29.4). Microspheres were fabricated by sonicating with high-intensity ultrasound the interface between a 5% weight per volume solution of BSA and a solution containing the material to be incorporated into the shell or encapsulated in the core. The high-intensity ultrasound necessary for the reaction was generated by a titanium horn with tip diameter of 1.25 cm, driven at 20 kHz (Figure 29.1). The solutions were sonicated for 3 minutes at an acoustic power of ~ 80 W/cm^2. The diameter of the microsphere is dependent on the acoustic power and the frequency of ultrasound. Solutions of microspheres were washed with nanopure water and filtered to remove fragments. A size range of 0.2–2 μm was selected to enable microspheres to pass readily through the microcirculation. Microspheres were re-suspended in nanopure water and, to prevent settling during optical characterization, were mixed with warmed liquid agarose and allowed to solidify. Average size, size distributions and initial concentrations (average 1.1×10^{10} microspheres/ml) were determined by Coulter Multisizer II analysis of each sample. Scanning and transmission electron micrographs of a representative contrast agent with an oil-filled core and scattering nanoparticles embedded in the shell are shown in Figure 29.4. The transmission electron micrograph demonstrates that the shell is composed of essentially a monolayer of scattering nanoparticles. For later optical characterization studies[17], the optical properties of three types of contrast agent were investigated for OCT by incorporating melanin, gold and carbon nanoparticles into the shell of oil-filled microspheres. These nanoparticles were chosen to provide a high degree of optical scattering, compared to biological tissue. Comparisons are also made with oil-filled contrast agents without shell nanoparticles. The encapsulation of vegetable oil as a core material made the contrast agents more stable and robust compared to air-filled microbubbles, extending their lifetime in solution to as long as several months.

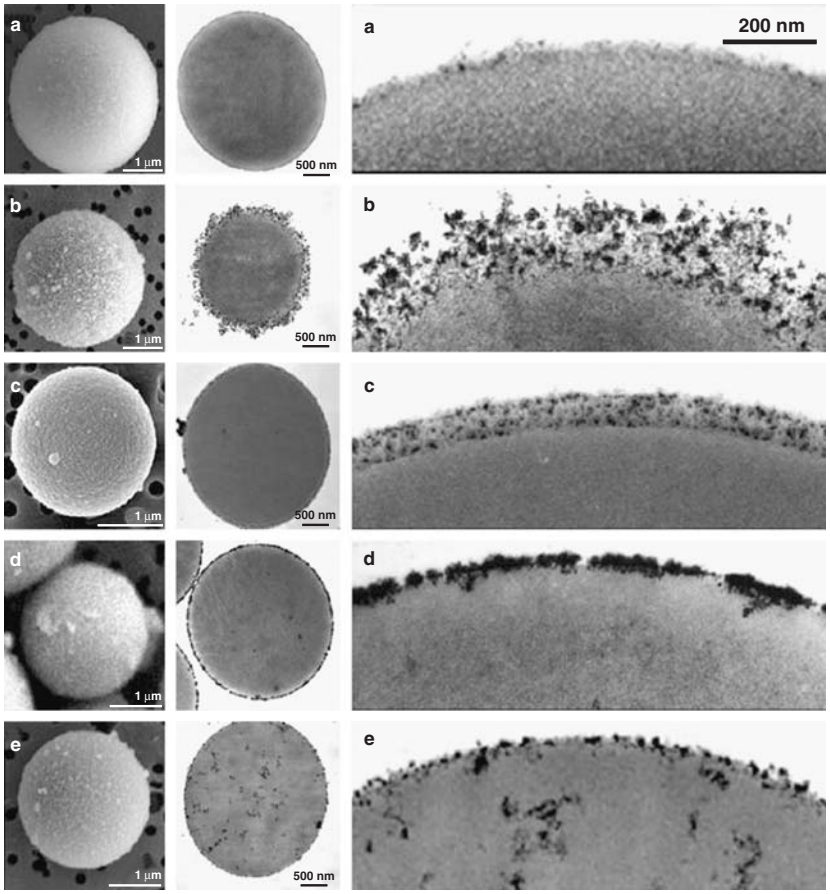

Figure 29.4 Surface modification of protein microspheres and microcapsules with nanocolloids. Scanning electron micrographs (left column) and transmission electron micrographs (TEMs) (middle column) of single microspheres. High-magnification TEMs (right column) of surface and shell structures are shown for unmodified bovine serum albumin protein-shelled microspheres (A), outer surface modified with gold nanoparticles (B), protein shell modified by pre-attachment of gold nanoparticles (C), protein shell modified by hydrophilic iron oxide nanoparticles (D) and interior core containing a hydrophobic iron oxide colloid (E). Modified figure reprinted with permission from reference 34

SURFACE MODIFICATION

The preparation of protein-shell microspheres is now well established. While essentially complete control over the interior core of the microsphere is possible, until very recently there has been limited control over the exposed surface. Since it is this surface that determines the pharmacokinetics (i.e. targeting)

of the protein-shell microspheres, recent efforts have been focused on surface modification. Approaches to this problem have included several different strategies such as conventional bioconjugation with covalent surface modification, and nanoparticle modification of protein-shell microspheres by strong adhesion of inorganic or organic nanoparticles to the shell proteins.

Bioconjugation with covalent surface modification

With protein-shell microspheres, one can chemically modify the shell using standard techniques to increase the microspheres' circulation time and to target specific organs. The surface modifications can be easily made using standard conjugation techniques, e.g. dextran-coated charcoal (DCC) amidation of protein surface amines, etc. This standard surface modification alters the pharmacokinetics and biodistribution of these microspheres *in vivo*.

Towards that goal, polyethylene glycol (PEG) chains have been attached. It has been found that this surface modification substantially extends the circulation time of the protein-shell microspheres before their removal by the liver and spleen. Following published procedures[33], the outer protein shell of serum albumin microspheres with a n-C_9F_{20} core has been modified. Rats were given intravenous injections of PEGylated and standard microspheres. Blood samples were taken via jugular vein cannulation at various time intervals. The n-C_9F_{20} microsphere concentration was estimated using high-resolution fluorine magnetic resonance (NMR) of equal volume samples. The measured circulation half-life of non-modified microspheres is approximately 5 minutes, while PEGylation extends this to more than 70 minutes.

Nanoparticle modification of protein-shell microsphere surfaces

A second approach to surface modification of the protein-shell microspheres involves the strong adhesion of inorganic or organic nanoparticles to the proteins of the protein-shell microsphere shell[34]. Several general methods for modifications of protein microspheres have been demonstrated using a variety of nanoparticles, both inorganic and organic. In addition, a general set of methods for the inclusion of nanoparticles into the outer surface, the protein shell, or the interior core of albumin protein microspheres has been developed. These modified protein microspheres have subsequently been used as contrast agents for OCT and magnetic resonance imaging. With these modifications, non-fluorescent optical contrast agents have been created for OCT. Additionally, the iron-oxide-modified microspheres are also excellent contrast agents for magnetic resonance imaging.

Specifically, nanoparticles of gold, iron-oxide, carbon, melanin and semiconductor quantum dots are of interest for various bioimaging modalities. Only the semiconductor quantum dots have proved to have significant toxicity. These nanoparticles are all readily available, and in separate work some extremely facile sonochemical routes to these nanoparticles have been developed[35–39].

Because the surface area/volume ratio is so large for particles below 5 nm, adsorption of small nanoparticles onto protein molecules is essentially irreversible. Surface electrostatics, ligation to surface atoms, hydrogen bonding and van der Waals interactions all contribute. Using a general set of methods for the inclusion of nanoparticles onto the outer surface, embedded within the protein shell, or contained within the interior core of albumin protein microspheres, a wide range of engineered microspheres have been developed. Figure 29.4 shows a selection of these results.

SURFACE FUNCTIONALIZATION FOR CELL TARGETING

The targeting of drugs to specific organs or classes of cells is of critical importance to future advancement of pharmaceutical applications. These microspheres/microcapsules are nearly ideally suited to act not only as diagnostic contrast agents, but also as therapeutic agents. They are robust, have long shelf-lives, can carry a substantial dose and have easily modified surfaces.

A general goal of ongoing work in this area is to develop synthetic methodologies for surface modification of the protein microspheres so as to alter the physical and chemical properties of the microspheres/microcapsules for nearly any appropriate imaging or targeting modality, including OCT. More specifically, for cellular targeting, a central aim is to modify microsphere surfaces with organ-specific or cancer cell-specific ligands and to observe the effect on the biodistribution and pharmacokinetics of the microspheres and their contents. Of particular interest is the modification of the microsphere surface with folate in order to target folate-binding tumor cells, and with arginine–glycine–aspartic acid (RGD) peptides to target integrin receptor-containing cells in atherosclerosis or angiogenesis. Towards these goals, it is possible to attach PEG chains (to extend their lifetime in the blood pool), membrane receptor ligands (e.g. folate, hemes, steroids, neurotransmitters), bioactive peptides and even antibody chains.

Integrin receptors

Integrin receptors are heterodimer, transmembrane receptors that have a wide range of functions: cell survival, migration, proliferation, differentiation and death. Recently, these receptors have been shown to play a key role in atherosclerosis, angiogenesis, cancer metastases and tumorigenesis. There are over 25 known integrin receptors, and most of these recognize the small tripeptide turn sequence (RGD)[40]. Integrin receptors are overexpressed in several pathological cell and tissue types. For example, the RGD tripeptide motif has been used as a label for tumor cells and their angiogenic vasculature[40].

In one effort to label BSA microspheres with integrin receptors[41], a layer-by-layer approach was used, and three different peptides were synthesized with an RGD motif embedded at the ends or in the middle of a highly positively charged, polylysine sequence: at the amino terminus, RGDKKKKKK; in the middle,

KKKKRGDKKK; and at the carboxy terminus, KKKKKKKRGD. The positively charged lysine residues electrostatically secure the RGD motif to the surface of the microspheres. An additional decapeptide polylysine, K10, was prepared as a control. These peptides were synthesized using standard Fmoc peptide chemistry by solid-phase peptide synthesizer, purified using high-pressure liquid chromatography (HPLC), and characterized by MALDI-TOF-MS.

Preliminary *in vitro* results have been obtained for these RGD small peptides bound to the outer surface of BSA microspheres. They are very effective in causing the phagocytosis of these microspheres into HT29 colon carcinoma cells, as shown by fluorescence microscopy in Figure 29.5. In spite of these very promising results, it is believed that the binding can still be substantially improved. The most tightly bound is RGDKKKKKK, but a longer sequence, with a few neutral residues linking the terminal RGD to a longer polylysine sequence might well improve the binding substantially. Quantitative binding studies are clearly a priority in future rounds of target peptide design.

OPTICAL CHARACTERIZATION

Scattering microspheres were fabricated using a 20-kHz ultrasound probe placed at the interface between liquids where high-energy ultrasound waves produce cavitation and microsphere formation. This fabrication protocol enables a wide range of flexibility in combining core, shell and surface composition, as listed in Table 29.1. Since scattering increases with the magnitude of the refractive index change, the use of metals or other materials with an index significantly different from tissue is desirable. Quantitative analysis of optical absorption and scattering properties of engineered microspheres demonstrated that the use of highly scattering nanoparticles of gold, melanin, carbon and iron-oxide produce strong scattering in OCT[17].

The refractive indices at 800nm, the center wavelength of a common titanium:sapphire laser OCT optical source, were obtained from the literature for bulk melanin, gold and carbon (Table 29.2). The refractive indices of the encapsulated oil (n=1.47), the agarose gel (n=1.34) and the four types of sample were also measured using OCT. For all contrast agent samples, refractive indices were within experimental error (5%) of the index of pure agarose due to the small fractional volume of the microspheres. The reduced scattering coefficients of the contrast agents (average concentration of 2.8×10^9 microspheres/ml) were determined with oblique-incidence reflectometry[42] using an 800-nm laser diode. This method was chosen to characterize thick preparations and will allow for *in situ* measurement of reduced scattering coefficients simultaneously with OCT. The oil-filled agents containing melanin, carbon and gold nanoparticles in the shell exhibited higher reduced scattering coefficients compared to microspheres without scattering nanoparticles. Upper limits of the absorption coefficients were measured for the contrast agents (average concentrations of 3.1×10^7 microspheres/ml) using a spectrophotometer (Thermo

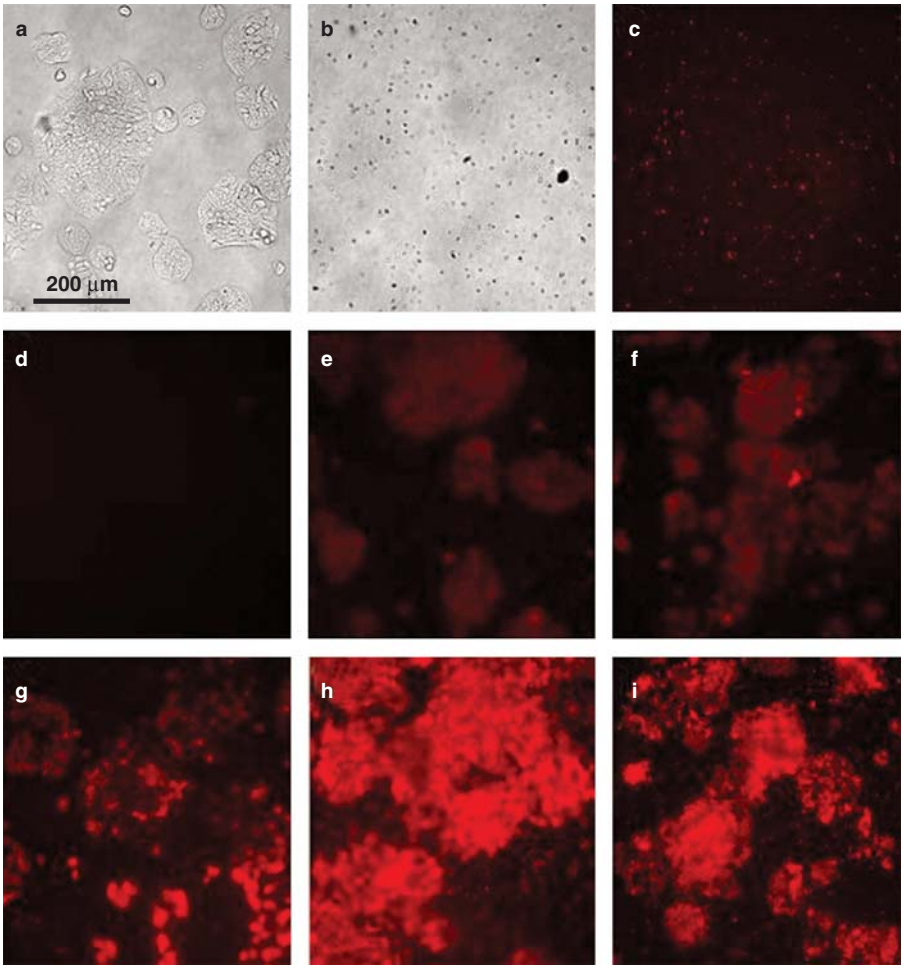

Figure 29.5 Targeted microspheres. Uptake of fluorescently labeled microspheres into the cell interiors of HT29 tumor cells. (A) Bright-field microscopy of cells and (B) fluorescently-labeled microspheres containing the dye Nile Red. Fluorescent microscopy images of fluorescent microspheres (C), cells (D), cells exposed to unlabeled microspheres (E), cells exposed to K_{10}-coated microspheres (F), cells exposed to K_4RGDK_3-labeled microspheres (G), cells exposed to $RGDK_6$-labeled microspheres (H) and cells exposed to K_7RGD-labeled microspheres (I). Figure reprinted with permission from reference 41

Spectronic 20). All agents exhibited low absorption coefficients as expected for these near-infrared wavelengths. Microsphere concentrations obtained from Coulter Multisizer II measurements and an approximated anisotropy coefficient of 0.8, based on microsphere size, were used to calculate scattering and absorption cross sections.

Table 29.2 Optical properties and characterization of protein microspheres with various nanoparticles embedded in the shell. Reprinted with permission from reference 17

Contrast agent	*Microsphere diameter (μm)*	*Refractive index*	*Reduced scattering coefficient (cm^{-1})*	*Absorption coefficient (cm^{-1})*	*Scattering x-section (cm^2) per sphere*	*Absorption x-section (cm^2) per sphere*
Oil	1.61 ± 0.72	1.47	10.8 ± 1.4	0.26 ± 0.01	2.22×10^{-8}	9.4×10^{-9}
Melanin	1.99 ± 0.99	1.66[44]	18.3 ± 3.6	0.45 ± 0.02	2.33×10^{-8}	1.0×10^{-8}
Gold	1.85 ± 0.79	0.18[45]	15.2 ± 4.1	0.69 ± 0.03	4.70×10^{-8}	3.8×10^{-8}
Carbon	1.66 ± 0.66	3.08[45]	19.9 ± 4.3	0.51 ± 0.03	3.26×10^{-8}	1.5×10^{-8}

Values are mean ± standard deviation, $n = 30$ measurements.

These results quantify the increased optical scattering of microspheres with various scattering nanoparticles embedded in the shell. These engineered microspheres were subsequently used in a three-layer agarose tissue phantom to demonstrate the scattering and contrast enhancement. The tissue phantoms consisted of three layers prepared by dispersing 400 mg of agarose in 25 ml of skim milk and 100 ml of water to reach a scattering coefficient approximating that for soft tissues. The middle layer of the phantom was additionally doped with various microsphere contrast agents at typical concentrations of 2.8×10^9 microspheres/ml. Figure 29.6 shows OCT images of these phantoms, using a fiber-based time-domain OCT system with a titanium : sapphire laser as the optical source. With uniform incident power of 6 mW on the phantoms, the OCT image containing the gold-modified microspheres (Figure 29.6F) exhibited the strongest optical backscatter, and all the other phantoms containing modified microspheres exhibited increased scattering relative to the control (no microspheres, Figure 29.6A) and relative to the phantom with unmodified microspheres (Figure 29.6B).

IN VIVO APPLICATIONS

To demonstrate the effects of these microsphere contrast agents on OCT images and in tissue, OCT was performed following the intravenous injection of gold-shelled contrast agents in a mouse animal model. The fiber-based OCT system used a Nd : YVO_4-pumped titanium : sapphire laser (Lexel Laser, Inc.) as a broadbandwidth optical source which produced 500 mW average power and approximately 90 fs pulses with an 80 MHz repetition rate at 800 nm center wavelength. Laser output was coupled into an ultrahigh numerical aperture fiber (UHNA4, Thorlabs, Inc.) to spectrally broaden the light from 20 nm to over 100 nm, increasing the axial resolution of our system[43] from 14 μm to 3 μm. The ultrahigh numerical aperture fiber was spliced directly to the single mode fiber of a broadband

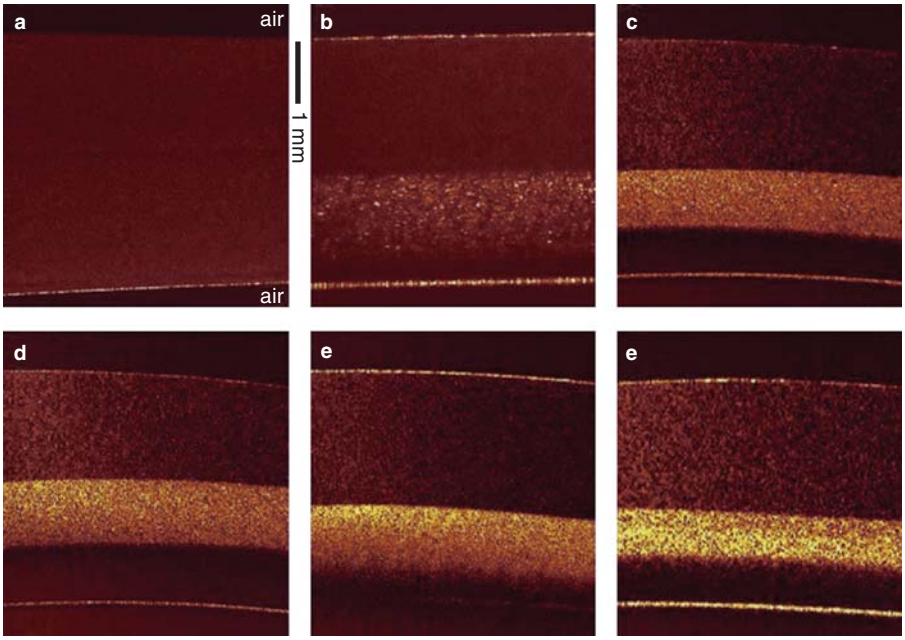

Figure 29.6 OCT of microspheres in three-layer tissue phantoms. (A) OCT of three-layer tissue phantom without microspheres. (B) Tissue phantom with oil-filled (no nanoparticles) protein microsphere layer (central band). (C) Microspheres with outer surface modified with melanin nanoparticles. (D) Microspheres with outer surface modified with carbon nanoparticles. (E) Microspheres with core containing Fe_2O_3 nanoparticles. (F) Microspheres with shell containing gold nanoparticles. Modified figure reprinted with permission from reference 34

50 : 50 fiber coupler (Gould Fiber Optics). The reference arm of the OCT interferometer contained a galvanometer-driven retroreflector delay line that was scanned a distance of 3 mm at a rate of 30 Hz. The sample arm beam was focused into the tissue by a 12.5 mm-diameter, 30-mm focal length achromatic lens to a 10 μm-diameter spot size (transverse resolution). The 6 mW beam was scanned over the tissue with a galvanometer-controlled mirror. The envelope of the interference signal was digitized to 12-bit accuracy.

OCT imaging was performed on Swiss mice (6-week-old, 27-g males) with and without contrast agents. In one study, mice were anesthetized by inhalation from halothane-soaked gauze. The liver was exposed for OCT imaging by shaving of the abdomen, making a mid-line incision, and reflecting back the abdominal skin and peritoneal wall. The liver was imaged because this is one end-organ site for collection of these non-targeted contrast agents as they are broken down and cleared. A 130 μl volume (6.5×10^9 microspheres/ml concentration) of oil-filled contrast agents with gold nanoparticles embedded in the shell was injected via a tail vein. OCT of surgically exposed liver was

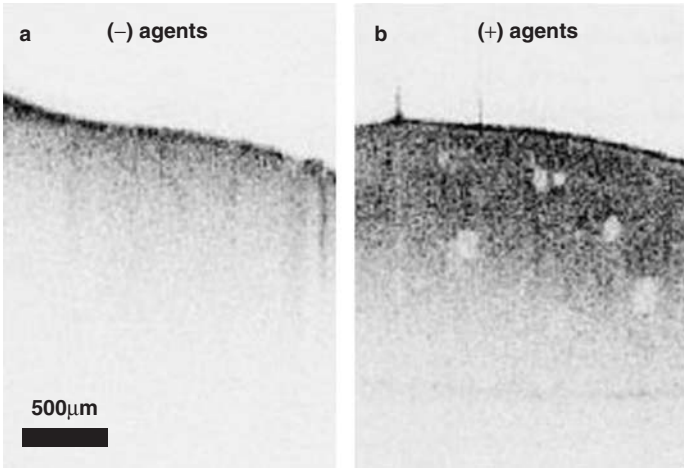

Figure 29.7 Protein microspheres as OCT contrast agents. OCT images of an *in vivo* mouse liver before and after tail-vein injection of gold-coated protein microspheres. Post-administration of the contrast agents reveals increased scattering from the liver, where Kuppfer cells had phagocytosed the scattering microspheres. The low-scattering regions are probably the liver vasculature. Modified figure reprinted with permission from reference 17

performed 20 minutes after injection and following euthanasia. OCT imaging was also performed on surgically exposed liver from control mice without contrast agents. Intravenous injection is one possible route for delivering these contrast agents to living tissue. Other routes include topical administration and direct injection into a tissue site. Figure 29.7 shows OCT images acquired from the exposed peritoneal surface of the liver. The OCT image acquired from a control mouse shows little subsurface structure. A change in scattering is readily apparent in the image acquired following the intravenous injection of the contrast agent. More structural detail, including liver sinusoids, is shown at greater depths in the contrast agent-enhanced liver image.

The administration of these engineered microspheres does provide dynamic scattering changes within tissue. Following mouse tail-vein injection of microspheres containing iron-oxide colloid in the core, and iron-oxide nanoparticles embedded in the shell, transient regional scattering changes were observed during imaging of the exposed mouse intestinal wall (Figure 29.8). Scattering variations were noted around a vascular region while minimal changes were observed in an avascular region immediately after the administration of the agents. While the larger microspheres are likely to remain in the vascular system because of their size, it remains to be determined whether the observed scattering changes were due to extravasation of smaller microspheres, degraded microsphere fragments, or a local accumulation of microspheres within the vascular system.

The primary mechanism of uptake of these non-targeted microspheres in the liver (Figure 29.7) was via phagocytosis by the resident macrophages (Kuppfer

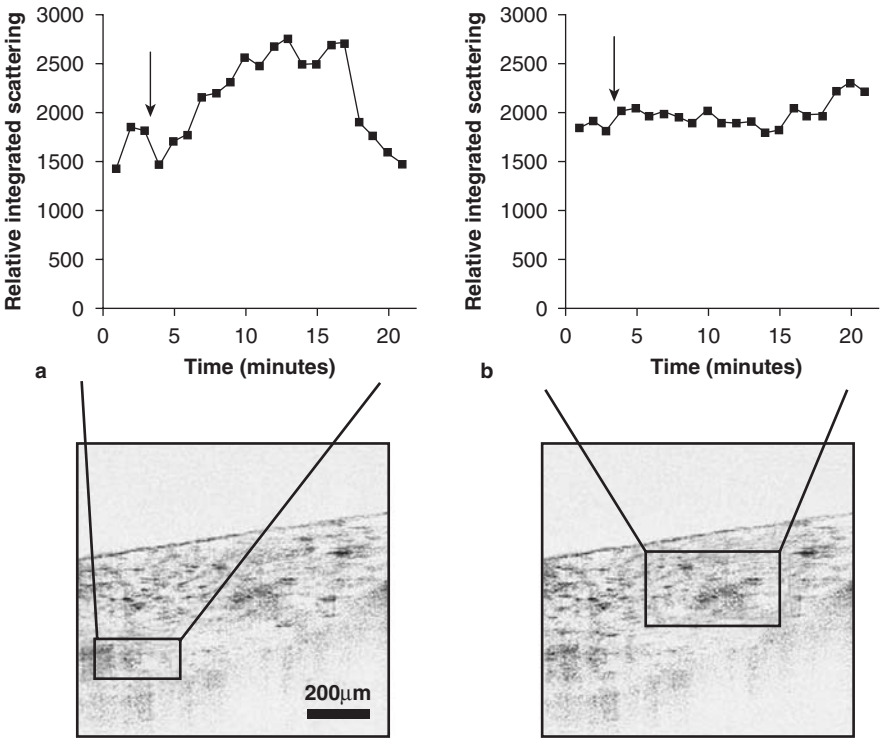

Figure 29.8 Dynamic scattering changes in tissue. Scattering changes within OCT images are noted following tail-vein injection of iron-oxide-encapsulated microspheres. OCT images were acquired from the exposed mouse intestinal wall at locations corresponding to vascular (left) and avascular (right) regions. The arrows indicate the time of contrast agent injection. Modified figure reprinted with permission from reference 15

cells). Transmission electron micrographs of *in vitro* macrophages (Figure 29.9) with and without exposure to microspheres show clearly that the microspheres are readily phagocytosed and broken down within these cells. In addition, iron-oxide-containing microspheres are readily visualized with TEM from liver tissue, and confirmed with Prussian-blue histological staining (Figure 29.9). Early *in vitro* cell viability studies have shown that these engineered microspheres have little to no cellular toxicity (JR Gunther *et al.*, unpublished data).

CONCLUSIONS

The flexibility of altering the scattering properties (and equally the absorption properties) of these microspheres is high, and the potential exists for these probes to be highly multifunctional. The protein-based shell of the microspheres

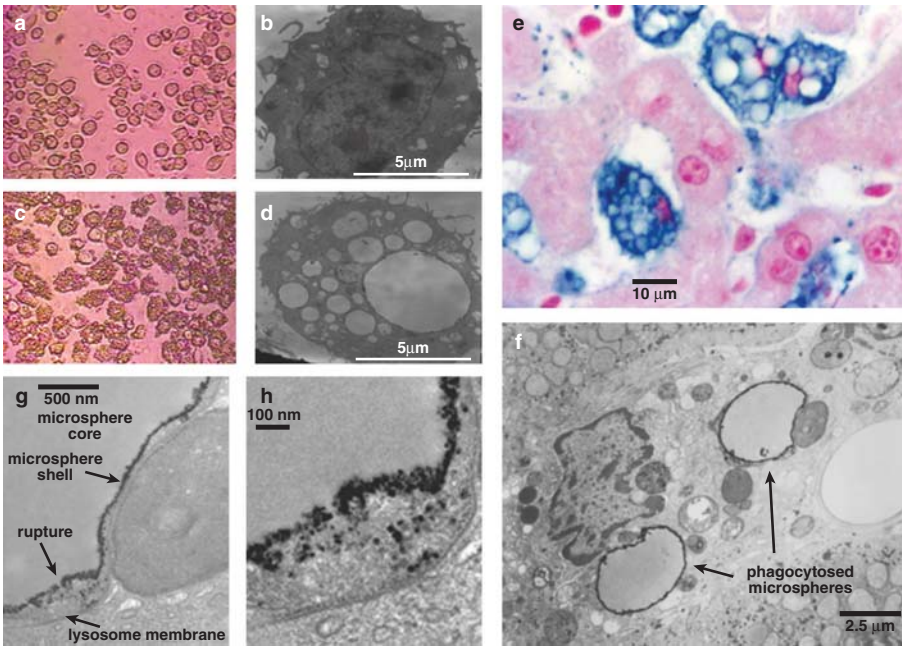

Figure 29.9 Cell interactions with microspheres. (A,B) Light microscopy and TEM of *in vitro* control macrophages (no exposure to microspheres). (C,D) Light microscopy and TEM of *in vitro* macrophages exposed to microspheres, showing phagocytic inclusions of microspheres. (E) Histology section of rat liver with Prussian blue staining following intravenous injection of iron-oxide nanoparticle-modified microspheres. The blue circular objects are the modified BSA microspheres, found in the liver sinusoids. (F,G,H) TEMs of sectioned liver macrophages at various magnifications showing digestion of iron-oxide modified microspheres. (G,H) A single microsphere shell is shown inside a phagosome after phagocytosis, and after release of the iron oxide nanoparticles (small black dots)

is readily functionalized, as has been demonstrated in ultrasound imaging[26], and for these engineered microspheres[41]. With the increasing number of viable molecular targets available, such as the overexpression of cell-surface receptors in states such as inflammation, atherosclerosis and cancer, it will be possible similarly to target these microspheres to molecularly specific sites *in vivo*. The physical size of these microspheres (1–3 μm average) prohibits their use as an agent that will extravasate from the intravascular space into the extravascular and extracellular spaces. Their use as a blood pool agent would be feasible for defining normal or angiogenic vascular networks, identifying regions of altered perfusion, or for labeling regions of vessels expressing specific markers during disease processes. Their relatively large size, however, is advantageous as a drug delivery vehicle, by encapsulating sufficient drug dosages to be delivered to specific sites. The engineered microsphere enables the fabrication of a scattering

(absorbing) contrast agent that uses selected nanoparticles spatially oriented on the microsphere shell, or within the core material, to optimize the scattering (absorption) cross section, whereby the use of nanoparticles alone, although smaller in size, are not likely to alter the local scattering (absorption) property of the tissue as strongly.

The diverse fabrication combinations and the large number of potential applications for these microsphere/microcapsule contrast agents has only begun to be explored. For clinical application a number of safety issues still have to be clarified. It is clear, however, that the use of these novel agents will expand the diagnostic ability of OCT, with the future potential of enabling highly site-specific labeling of cells and tissues at the molecular level, making molecular OCT imaging clinically feasible.

ACKNOWLEDGMENTS

We wish to thank our students, research scientists and colleagues for advancing this research, including Dr Kenneth J Kolbeck, Dr Daniel Marks, Dr Amy Oldenburg, Dr Farah Jean-Jacques Toublan, and Wei Luo. All animals used in this study were cared for under protocols approved by the Institutional Animal Care and Use Committee from the University of Illinois at Urbana-Champaign. This work was supported in part by grants from The Whitaker Foundation (S.A.B.), the American Heart Association (0355396Z, S.A.B.), and the National Institutes of Health (1 R21 EB005321A, S.A.B., HL25934, K.S.S.). Additional information can be found at: http://biophotonics.uiuc.edu.

REFERENCES

1. Klibanov AL. Targeted delivery of gas-filled microspheres, contrast agents for ultrasound imaging. Adv Drug Deliv Rev 1999; 37: 139–57
2. Gazelle GS, Wolf GL, McIntire GL, et al. Nanoparticulate computed tomography contrast agents for blood pool and liver–spleen imaging. Acad Radiol 1994; 1: 373–6
3. Su MY, Muhler A, Lao X, et al. Tumor characterization with dynamic contrast-enhanced MRI using MR contrast agents of various molecular weights. Magn Reson Med 1998; 39: 259–69
4. Weissleder R, Ntziachristos V. Shedding light onto live molecular targets. Nat Med 2003; 9: 123–8
5. Huang D, Swanson EA, Lin CP, et al. Optical coherence tomography. Science 1991; 254: 1178–81
6. Fujimoto JG. Optical coherence tomography for ultrahigh resolution in vivo imaging. Nat Biotech 2003; 21: 1361–7
7. Schuman JS, Puliafito CA, Fujimoto JG. Optical Coherence Tomography of Ocular Diseases. New Jersey: Slack, 2004
8. Bouma BE, Tearney GJ. Handbook of Optical Coherence Tomography. New York: Marcel Dekker, 2001

9. Tearney GJ, Brezinski ME, Bouma BE, et al. In vivo endoscopic optical biopsy with optical coherence tomography. Science 1997; 276: 2037–9
10. Boppart SA, Bouma BE, Pitris C, et al. In vivo cellular optical coherence tomography imaging. Nat Med 1998; 4: 861–5
11. Jang IK, Tearney GJ, MacNeill B, et al. In vivo characterization of coronary atherosclerotic plaque by use of optical coherence tomography. Circulation 2005; 111: 1551–5
12. Winter PM, Morawski AM, Caruthers SD, et al. Molecular imaging of angiogenesis in early-stage atherosclerosis with alpha(v)beta3-integrin-targeted nanoparticles. Circulation 2003; 108: 2270–4
13. Antonov AS, Kolodgie FD, Munn DH, et al. Regulation of macrophage foam cell formation by alphaVbeta3 integrin: potential role in human atherosclerosis. Am J Pathol 2004; 165: 247–58
14. Schmieder AH, Winter PM, Caruthers SD, et al. Molecular MR imaging of melanoma angiogenesis with $\alpha_v\beta_3$-targeted paramagnetic nanoparticles. Magn Res Med 2005; 53: 621–7
15. Boppart SA, Oldenburg AL, Xu C, et al. Optical probes and techniques for molecular contrast enhancement in coherence imaging. J Biomed Opt 2005; 10: 041208
16. Barton JK, HoyingJB, Sullivan CJ. Use of microbubbles as an optical coherence tomography contrast agent. Acad Radiol 2002; 9S: 52–71
17. Lee TM, Oldenburg AL, Sitafalwalla S, et al. Engineered microsphere contrast agents for optical coherence tomography. Opt Lett 2003; 28: 1546–8
18. Yang C, McGuckin LE, Simon JD, et al. Spectral triangulation molecular contrast optical coherence tomography with indocyanine green as the contrast agent. Opt Lett 2004; 29: 2016–18
19. Xu C, Ye J, Marks DL, et al. Near-infrared dyes as contrast-enhancing agents for spectroscopic optical coherence tomography. Opt Lett 2004; 29: 1647–9
20. Chen J, Saeki F, Wiley BJ, et al. Gold nanocages: bioconjugation and their potential use as optical imaging contrast agents. Nano Lett 2005; 5: 473–7
21. Loo C, Lin A, Hirsch L, et al. Nanoshell-enabled photonics-based imaging and therapy of cancer. Technol Cancer Res Treat 2004; 3: 33–40
22. Oldenburg AL, Toublan FJJ, Suslick KS, et al. Magnetomotive contrast for in vivo optical coherence tomography. Opt Express 2005; 13: 6597–614
23. Liu KJ, Grinstaff MW, Jiang J, et al. In vivo measurement of oxygen concentration using sonochemically synthesized microspheres. Biophys J 1994; 67: 896–901
24. Christiansen C, Kryvi H, Sontum PC, et al. Physical and biochemical characterization of Albunex, a new ultrasound contrast agent consisting of air-filled albumin microspheres suspended in a solution of human albumin. Biotechnol Appl Biochem 1994; 19: 307–20
25. Geny B, Piquard F, Muan B, et al. Contrast echocardiology in coronary artery disease patients: effect of systemic and pulmonary artery pressures on left heart opacification after intravenous injections of Albunex. Coron Artery Dis 1997; 8: 77–81
26. Lindner JR. Evolving applications for contrast ultrasound. Am J Cardiol 2002; 90: 72J–80J
27. Horisberger M. Colloidal gold: a cytochemical marker for light and fluorescent microscopy and for transmission and scanning electron microscopy. Scanning Electron Micros 1981; 11: 9–31
28. Suslick KS, Grinstaff MW. Protein microencapsulation of nonaqueous liquids. J Am Chem Soc 1990; 112: 7807–9

29. Grinstaff MW, Suslick KS. Air-filled proteinaceous microbubbles: synthesis of an echo-contrast agent. Proc Natl Acad Sci USA 1991; 88: 7708–10
30. Jocelyn PC. The Biochemistry of the SH Group. New York: Academic Press, 1972
31. Flannigan DJ, Suslick KS. Plasma formation and temperature measurement during single-bubble cavitation. Nature 2005; 434: 52–5
32. Suslick KS, Didenko Y, Fang MM, et al. An acoustic cavitation and its chemical consequences. Phil Trans R Soc Lond 1999; 357: 335–53
33. Roberts MJ, Bentley MD, Harris JM. Chemistry for peptide and protein PEGylation. Adv Drug Deliv Rev 2002; 54: 459–76
34. Toublan FJJ, Kolbeck KJ, Oldenburg AL, et al. Nanoparticle modification of core-shell protein microcapsules. J Am Chem Soc 2005; submitted
35. Suslick KS, Price G. Applications of ultrasound to materials chemistry. Annu Rev Matl Sci 1999; 29: 295–326
36. Suh WH, Suslick KS. Magnetic and porous nanospheres from ultrasonic spray pyrolysis. J Am Chem Soc 2005; 127: 12007–10
37. Didenko YT, Suslick KS. Chemical aerosol flow synthesis of semiconductor nanoparticles. J Am Chem Soc 2005; 127: 12196–7
38. Suslick KS, Fang M, Hyeon T. Sonochemical synthesis of iron colloids. J Am Chem Soc 1996; 118: 11960–1
39. Skrabalak SE, Suslick KS. Porous MoS_2 synthesized by ultrasonic spray pyrolysis. J Am Chem Soc 2005; 127: 9990–1
40. Hwu P, Du MX, Lapointe R, et al. Indolamine 2,3-dioxygenase production by human dendritic cells results in the inhibition of T cell proliferation. J Immunol 2000; 164: 3596–9
41. Toublan FJJ, Boppart SA, Suslick KS. Tumor targeting by surface modified protein microspheres. J Am Chem Soc 2005; in press
42. Wang L, Jacques SL. Use of a laser beam with an oblique angle of incidence to measure the reduced scattering coefficient of a turbid medium. Appl Opt 1995; 34: 2362–6
43. Marks DL, Oldenburg AL, Reynolds JJ, et al. Study of an ultrahigh-numerical aperture fiber continuum generation source for optical coherence tomography. Opt Lett 2003; 27: 2010–12
44. Vitkin A, Woolsey J, Wilson BC, et al. Optical and thermal characterization of natural (sepia officinalis) melanin. Photochem Photobiol 1994; 59: 455–62
45. Kurtz SK, Kozikowski SD, Wolfram LJ. Nonlinear optical and electro-optical properties of biopolymers. In: Gunther P, ed. Electro-Optics and Photorefractive Materials. Berlin: Springer-Verlag, 1986: 110–30